ÉCOLE POLYTECHNIQUE

PHY591 Research Internship

Fields, Particles and Matter

M1 High Energy Physics

Thomas LEPLUMEY

PMT Study and some Low-Energy Concerns

for Hyper-Kamiokande

March-July 2023

Supervisor :

Yasuhiro NISHIMURA, Keio University

Acknowledgements

I am deeply grateful to the following individuals and organizations who have played pivotal roles in making my internship experience both enriching and rewarding:

I extend my heartfelt gratitude to Prof. Yasuhiro Nishimura, my supervisor, for his warm welcome into his lab and unwavering guidance throughout the entirety of my internship. His mentorship and continuous support were instrumental in shaping my projects and in allowing me to explore various facets of the Hyper-Kamiokande collaboration. I am particularly thankful for the opportunities he provided, which enabled me to visit pertinent sites and present my work at the collaboration meeting.

I would like to express my sincere appreciation to my fellow students in the lab, whose camaraderie and assistance helped me seamlessly adapt to the Japanese way of life and facilitated my immersion into the culture of Japan.

I am indebted to Michel Gonin for his generous scholarship through the ILANCE laboratory. Additionally, I am thankful for the opportunity to attend the International Conference on the Physics of the Two Infinities, an event organized by him. His support significantly contributed to my academic pursuits.

I extend my thanks to Prof. Takuya Tashiro for overseeing my work in Kamioka and for his invaluable guidance on PMT hardware. His mentorship allowed me to gain hands-on experience within the context of the Hyper-Kamiokande construction, an endeavor that I found immensely insightful.

I would also like to express my gratitude to the diverse group of students and physicists I had the privilege of meeting during my time in Kamioka and the Hyper-Kamiokande collaboration meeting. Their enriching conversations, shared experiences, and camaraderie made each day memorable and significantly expanded my understanding of experimental physics.

Executive summary

French. Pour conclure ma première année de Master en Physique des Hautes Energies, j'ai intégré la collaboration Hyper-Kamiokande dans le cadre d'un stage de quatre mois au Japon. Découverte du monde de la physique des particules expérimentale, cette expérience m'a permis tant de comprendre l'organisation à grande échelle d'une collaboration comme Hyper-Kamiokande que d'assimiler des compétences dans de multiples tâches spécifiques. Tout d'abord, j'ai été initié aux enjeux matériels concernant les photo-détecteurs en allant moi-même en installer à Kamioka sur le site du détecteur et en analysant le signal ainsi récolté. Une étude du bruit généré à l'intérieur de ces appareils m'a permis de mettre en évidence et de comprendre des anomalies dans les mesures, qui menaçaient alors la production de masse pour la construction du détecteur. Qui plus est, un travail plus approfondi sur la dépendance en température du comportement de ces photo-détecteurs m'a permis d'établir un modèle utilisable en pratique, et que j'ai présenté au meeting international de la collaboration Hyper-Kamiokande. En parallèle, j'ai également été chargé d'explorer des techniques d'analyse de données pour du *neutron tagging* à basse énergie en utilisant de l'apprentissage automatique (*machine learning*). Ce travail s'est révélé moins fructueux que les précédents, en raison de nombreux problèmes techniques inattendus. Cela m'a amené à réorienter le projet pour en modifier l'objectif, permettant ainsi d'établir des bases pour de futures études sur le sujet en résolvant une partie des problèmes auxquels j'ai été confronté. Grâce à ce stage, je pense ainsi disposer d'une partie des clés nécessaires pour effectuer les choix qui s'imposeront dans la suite de ma carrière en recherche, notamment en ce qui concerne le doctorat.

English. To conclude my first year of a Master's program in High Energy Physics, I joined the Hyper-Kamiokande collaboration for a four-month internship in Japan. This experience introduced me to the world of experimental particle physics, allowing me to both grasp the intricacies of large-scale collaborations like Hyper-Kamiokande and acquire skills in various specific tasks. Firstly, I was introduced to the hardware challenges related to photo-sensors by personally installing them at the Kamioka detector site and analyzing the collected signals. An investigation into the noise generated within these devices enabled me to identify and comprehend anomalies in the measurements, which posed a threat to the mass production for the detector's construction. Furthermore, a more in-depth exploration of the temperature dependence of these photo-sensors' behavior led me to establish a practically usable model, which I presented at the international meeting of the Hyper-Kamiokande collaboration. In parallel, I was also tasked with exploring data analysis techniques for low-energy neutron tagging using machine learning. This endeavor proved to be less fruitful than the previous ones, due to numerous unexpected technical challenges. This prompted me to reshape the project and adjust its objectives, thereby laying the groundwork for future studies on the subject by addressing some of the issues I encountered. Thanks to this internship, I believe I now possess some of the essential tools to make informed decisions as I progress in my research career, particularly with regard to pursuing a PhD.

Contents

Introduction

As an essential part of my master studies in High Energy Physics, this four months internship in Japan was the opportunity to discover the experimental world in particle physics, by being deeply immersed into one of its major experiments: the neutrino observatory (currently under construction) Hyper-Kamiokande. While my initial aspirations did not lean toward hardware aspects of an experiment, I recognized the importance of gaining hands-on experience with the organization and operation of a large-scale international collaboration in particle physics. Consequently, I chose to work with Prof. Yasuhiro Nishimura at Keio University, a prominent figure in the Hyper-Kamiokande project. Additionally, having previously undertaken a project related to neutrino physics, I possessed a solid foundation in the theoretical context and experimental objectives of the field, enabling me to concentrate on more technical aspects.

During my time at Keio University, I undertook several projects as part of the Hyper-Kamiokande experiment, guided by Nishimura-san. One project centered on investigating the noise characteristics of Photo-Multiplier Tubes (PMTs), integral to the neutrino detector, enhancing my understanding of PMT hardware and associated practical challenges. Simultaneously, a data analysis project employing machine learning techniques allowed me to get used to the handling of Hyper-Kamiokande data at low energy. Concurrently, these two projects followed distinct paths. While the second one encountered challenges due to tool malfunctions and accreditation issues, leading me to adapt the objectives of the project, my research on PMT noise progressed smoothly and yielded valuable results that held significant implications for the collaboration, especially regarding PMT mass production. Additionally, I had the opportunity to enhance my understanding of the detector by visiting the Kamioka site, where I observed the electronics of Super-Kamiokande and participated in the installation of one hundred new PMTs, gaining valuable hands-on experience.

Furthermore, I sought to engage with experts across high-energy physics disciplines, and I achieved this by attending international meetings and conferences. Specifically, I reached out to Prof. Michel Gonin of the ILANCE laboratory, organizer of the 'International Conference on the Physics of the Two Infinities' in Kyoto during my internship's initial week. With generous support from ILANCE, I gained valuable insights into the latest developments in high-energy physics. Furthermore, as part of my ongoing efforts to integrate into the collaboration, I aimed to participate in the concluding Hyper-Kamiokande international collaboration meeting in July. To achieve this, I continued my research on PMT noise, securing unprecedented results regarding the temperature dependency of PMT behavior. This accomplishment allowed me to present my work at the collaboration meeting, marking a significant milestone in my internship.

In summary, my internship experience was not limited to a single project over the four months. Instead, I seized the opportunity to engage in conferences and meetings, work closely with the detector, and explore various facets of the collaboration. Consequently, although not all aspects naturally lend themselves to presentation in this report, the following chapters aim to present the conduct and outcomes of my projects throughout this internship.

Chapter 1

The Hyper-Kamiokande Project

This section aims to present the Hyper-Kamiokande project and its main stakes to non specialist readers. We will first present the main concept of Water Cherenkov Detector (WCD), which designates a category of detectors sharing the same global goals and methods. Then, we will describe the main physical phenomena implied in neutrino detection with this detector, that is, their different interactions with matter, and the Cherenkov Effect which allows good detection and reconstruction of incoming neutrinos. Finally, we will introduce the Photo-Multiplier Tubes (PMT) operating mode, which produce the raw signal of the detector.

1.1 Water Cherenkov Detectors (WCD)

A Water Cherenkov Detector (WCD) consists in a huge tank filled with pure water (and eventually a small proportion of additional components, e.g. Gadolinium), whose inner surface is covered with photo-sensors, that is, captors that can detect light with the precision of single photons. Such architecture allows some interactions or decays to happen in the water tank, and to be detected by the photo-sensors through their products.

Different architectures can exist for the tank, such as cylinders (e.g. Kamiokande, Super-Kamiokande, Hyper-Kamiokande), spheres (e.g. JUNO) or cubes (e.g. DUNE), see Figure 1.1. There are also different concepts, where the photo-sensors form a network inside the medium. Famous examples of such architectures are IceCube (in ice) and KM3NeT (in the sea), see Figure 1.2.

Figure 1.1: Photos inside the tank of Super-Kamiokande (left), JUNO (middle) and DUNE (right).

WCDs are particularly useful for detecting rare events, as the probability of observing these events is proportional to the volume of the tank. Therefore, the volume of the new WCDs tends to be larger and larger. Super-Kamiokande, which started operations in 1996, has a volume of

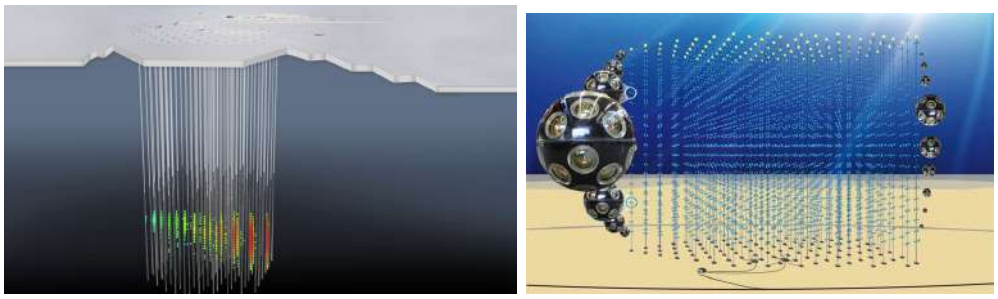

Figure 1.2: Schematic representations of IceCube (left) and KM3NeT (right).

50 millions cubic meters, and its successor under construction, Hyper-Kamiokande, will have a volume 20 times larger, of about 1 billion cubic meters.

The main particles these detectors are designed for are neutrinos, as these particles interact extremely few with matter, and are almost impossible to detect without a huge volume of matter. Furthermore, a huge interest in neutrinos has emerged in the last decades, with the discovery of neutrino oscillations (see Section 1.2.2). But other events are also searched in WCDs, such as proton decay (the initial goal of Kamiokande), an hypothetical event that would highlight new physics Beyond Standard Model.

1.2 Motivations of neutrino studies

In order to understand the interest in neutrino studies, some explanations are needed. We will mainly focus on two aspects of neutrino studies, which are supernova detection, and oscillation measurements.

1.2.1 Supernova detection

In simple terms, a supernova is a dying star explosion. In that process, a huge amount of photons is emitted, which allows optical detectors looking at the supernova to detect it and learn some information about the extreme processes happening during the explosion.

However, light is not the unique product of a supernova, and in particular, a huge amount of neutrinos is also emitted. Furthermore, because neutrinos interact much less with matter than photons, they are able to escape the supernova before them. Therefore, detecting these neutrinos, in addition to providing information about the supernova itself, can be used as a warning to orient the instruments in the right direction in order to observe the photons that will arrive later.

Unfortunately, this method can be used only for supernova happening close enough to us. So far, the only supernova that has been detected that way is SN 1987A, which was detected in 1987 at a distance of 168 000 light years from us.

1.2.2 Neutrino oscillations

A more recent discovery in the neutrino sector is the evidence of neutrino oscillations in 1998, which granted the Nobel prize to Takaaki Kajita and Arthur McDonald in 2015. This discovery has a very important impact in our understanding of neutrinos, as it proves that neutrinos have masses.

More precisely, in order to understand neutrino oscillations, one must know that neutrinos come in three different flavours : electronic neutrinos ν_e, muonic neutrinos ν_μ and tauic neutrinos ν_τ. These states of the neutrinos characterize which particles they can interact with (respectively electrons e^-, muons μ^- and tauons τ^-).

However, it was observed that when they propagate into space, neutrino flavours can change: a neutrino can oscillate between these different flavours. This can be explained by two new elements in the model: firstly, neutrinos need to have masses, and secondly, the mass (propagation) states are different than the flavour (interaction) states.

Let's introduce three mass states ν_1, ν_2 and ν_3, associated to three well-defined masses m_1, m_2 and m_3. The flavour states are then expressed as linear combinations of the mass states:

$$\begin{pmatrix} \nu_e \\ \nu_\mu \\ \nu_\tau \end{pmatrix} = U_{\text{PMNS}} \begin{pmatrix} \nu_1 \\ \nu_2 \\ \nu_3 \end{pmatrix}$$

The unitary matrix describing this transformation is called the Pontecorvo-Maki-Nakagawa-Sakata (PMNS) matrix. Thanks to the unitarity of this matrix, its 9 complex parameters can be reduced to 9 real parameters. Furthermore, given the global phases of the leptonic fields are not observable, 5 of these parameters can also be absorbed in these phases. Therefore, only 4 free real parameters remain, and the PMNS matrix is usually parameterized the following way:

$$U_{\text{PMNS}} = \begin{pmatrix} 1 & 0 & 0 \\ 0 & \cos\theta_{23} & \sin\theta_{23} \\ 0 & -\sin\theta_{23} & \cos\theta_{23} \end{pmatrix} \begin{pmatrix} \cos\theta_{13} & 0 & \sin\theta_{13}\, e^{-i\delta_{\text{CP}}} \\ 0 & 1 & 0 \\ -\sin\theta_{13}\, e^{i\delta_{\text{CP}}} & 0 & \cos\theta_{13} \end{pmatrix} \begin{pmatrix} \cos\theta_{12} & \sin\theta_{12} & 0 \\ -\sin\theta_{12} & \cos\theta_{12} & 0 \\ 0 & 0 & 1 \end{pmatrix}$$

The three angles θ_{12}, θ_{13} and θ_{23} are called the mixing angles, and they are related to the amplitudes of the different oscillation modes (whose frequencies are controlled by the squared mass differences Δm^2_{ij}), as seen in Figure 1.3. The phase δ_{CP} is called the CP violation phase (in the lepton sector), and is related to the matter/antimatter asymmetry concerning the lepton interactions.

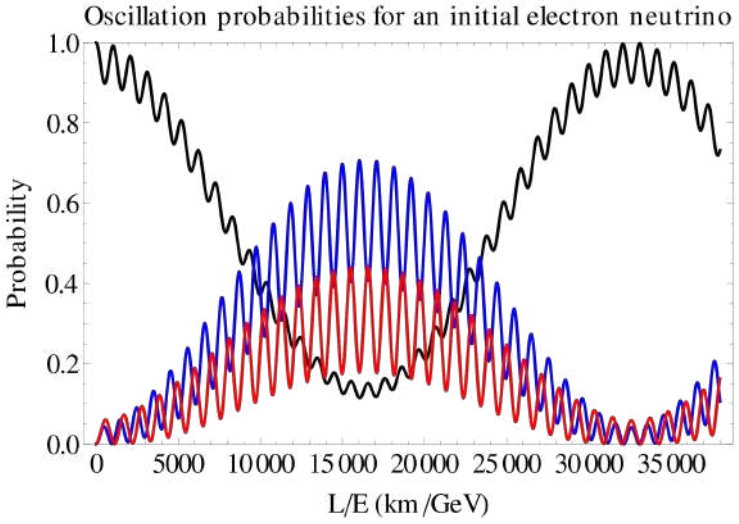

Figure 1.3: Oscillation probabilities for an initial electronic neutrino, as a function of the distance traveled L. The black curve stands for electronic neutrino, the blue for muonic neutrino and the red for tauic neutrino.

The measurement of all these parameters is another purpose of neutrino experiments. For example, the T2K experiment consists in throwing neutrinos to a far detector, that is Super-Kamiokande or Hyper-Kamiokande, in order to determine the parameters related to "low-frequency" oscillations (i.e. small difference of squared masses). On the other side, the analysis of solar neutrinos allows to determine the parameters related to "high-frequency" oscillations.

1.3 Neutrino interactions

In order to understand how neutrinos can be detected in a WCD, an explanation of their interactions with matter is needed. Actually, neutrinos are not directly detected in the experiment, as they do not interact enough to allow it. Instead, we let the neutrinos interact in the water tank, and the products of this interaction, mainly charged leptons $e^{\pm}$ and $\mu^{\pm}$, are detected via Cherenkov effect (explained in section 1.4).

There are different processes for neutrino interactions in water, that predominate at different energies. These processes are categorized in the following groups:

- Coherent Scattering: at low energy the neutrino just bounces off the nucleus.
- Quasi-Elastic Scattering (QE): at higher energies, the neutrino might be energetic enough to penetrate the nucleus and interact with the nucleons. There are two channels, interaction through charged current (CC) and neutral current (NC).

$$\begin{aligned} &\text{(CC)} \begin{cases} \overline{\nu}_l + p \rightarrow l^+ + n \\ \nu_l + n \rightarrow l^- + p \end{cases} \\ &\text{(NC)} \quad \nu_l + p(n) \rightarrow \nu_l + p(n) \end{aligned}$$

  The nucleon can be promoted to an excited state (Δ of different charges) by resonance (RES), which will eventually decay into pions. Charged pions can easily be confused with charged leptons in the detector, and must therefore be treated carefully.

- Deep Inelastic Scattering (DIS): at the highest energies, the neutrino breaks the nucleon and we end up with a hadronic shower in the final state, as well as a charged lepton.

Figure 1.4 shows the cross section (which is proportional to the probability of the process happening) of these different processes as function of the energy, for neutrinos and anti-neutrinos.

1.4 Cherenkov effect

Once a charged lepton is produced in the water tank, at the so called interaction vertex, this lepton will be detectable thanks to the so called Cherenkov effect, or Cherenkov radiation.

This effect can be understood as follows. As the incoming neutrino is highly energetic, it will transfer almost all its energy to the charged lepton (because it is the significantly lighter product of the interaction), and therefore this charged lepton will travel at a speed close to the speed of light (in vacuum) c. However, the actual speed of light in water, c_w, is lower than c (approximately $c_w \approx \frac{c}{1.33}$). Therefore, the radiation emitted by the charged lepton during its propagation in water will be emitted with a certain angle θ with respect to its direction, as shown in Figure 1.5.

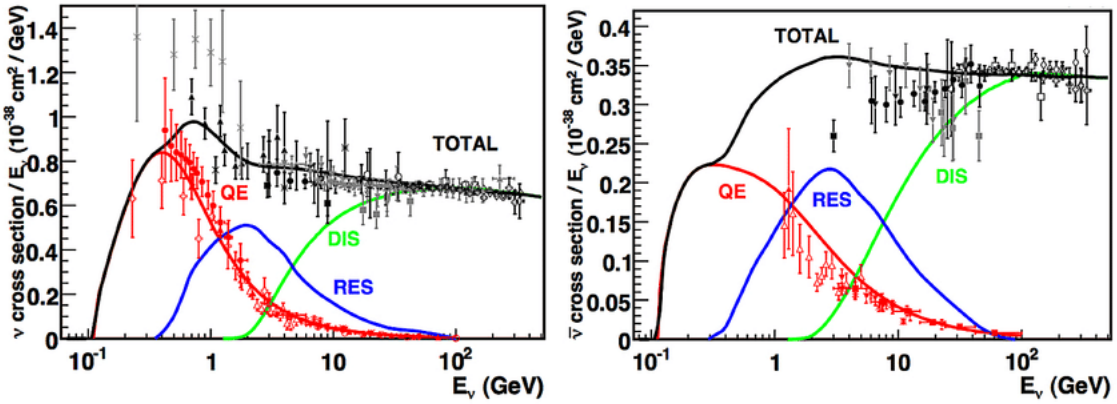

Figure 1.4: Cross-sections for the interaction of neutrinos and anti-neutrinos with nucleons as a function of the energy of the incoming neutrino [4].

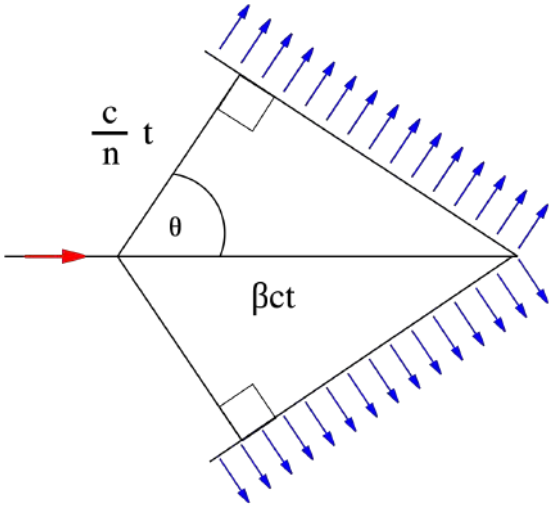

Figure 1.5: Cherenkov effect [11].

As it radiates, the charged lepton will loose its energy, until it completely slows down. At this point, the lepton will stop emitting Cherenkov light, and thus the overall emitted light has the shape of a cone, with a given thickness corresponding to the distance traveled by the lepton before being stopped. The cone will then be projected on the inner surface of the tank to be detected by the photo-sensors, forming a ring, called Cherenkov ring.

Examples of Cherenkov rings are represented in Figure 1.6.

1.5 Photo-Multiplier Tubes (PMT)

The final step of the detection process is the captation of Cherenkov light by the photo-sensors on the inner surface of the tank. One single photo-sensor is shown in Figure 1.7. In order to detect event with relatively low energy (the best we can do today is around $1MeV$), the photo-sensors have to be sensitive enough to detect single incoming photons, while the noise have to be low enough not to hide the signal.

This goal of sensitivity is achieved thanks to photomultiplier tubes, whose operating mode is described in Figure 1.8. The detection process can be decomposed in multiple steps:

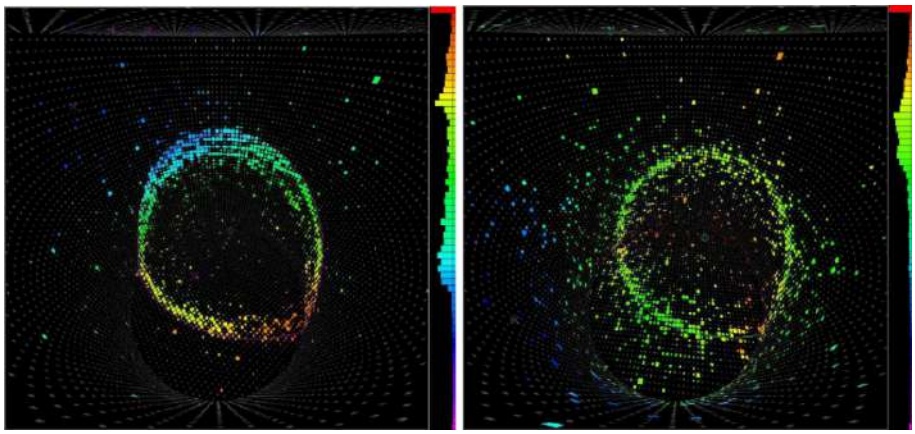

Figure 1.6: Cherenkov rings in the Super-Kamiokande inner detector. The color represents the time and the size represents the charge of the hits (c.f. Section 1.5). On the left, the very clean ring caused by a muon, and on the right, the much fuzzier ring caused by an electron, due to a more important impact of dispersion for a lighter particle.

Figure 1.7: Photo of a single photo-sensor for Hyper-Kamiokande.

- When a photon arrives at the photo-sensor, it will either be reflected by the glass (in that case no signal is generated), or penetrate inside the scintillator.
- In the scintillator, it will then ionize a gas to generate scintillation photons that will eventually hit the photocathode.
- By photoelectric effect, the photocathode will generate so called primary electrons.
- The primary electrons are accelerated by an electric field and will hit the first dynode.
- By secondary emission, more secondary electrons are emmitted by the first dynode, and will be accelerated by the electric field to hit the second dynode.
- This process continues recursively, so that in the end a large amount of secondary electrons hit the anode, leading to a measurable charge.

The PMT signal can then be seen as a series of values of voltage over time. However, although it would be more precise, acquisition of this full signal is impossible, as it would require too much storage. Instead, a basic analysis is made by the hardware itself in order to digitize and identify the hits in this signal in real time. Then, only the information of time and charge is conserved and stored each time a hit is identified.

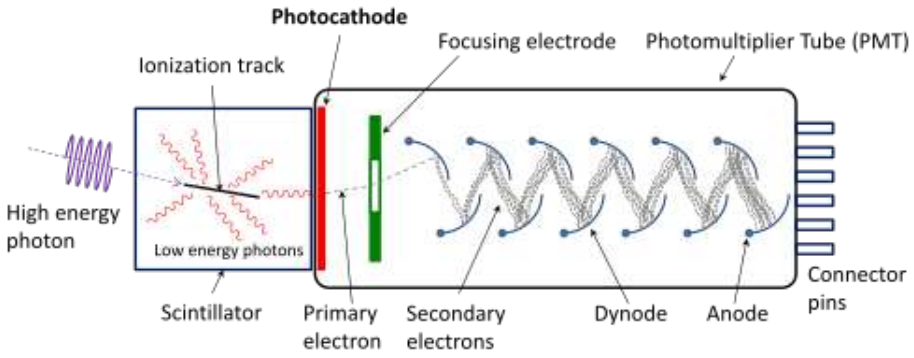

Figure 1.8: Operating process of a photo-multiplier tube.

At the end of this process, the information of time and charge for each hit of each PMT constitutes the raw data for the detector. One event (for example for an incoming neutrino) is then characterized by the collection of hits it generates, as we can see in Figure 1.6.

Chapter 2

PMT Dark Noise measurements and analysis

This second chapter aims to present the core subject of my research, which is the dark noise analysis for Hyper-Kamiokande PMTs. During this internship, I had the chance to work on many different aspects of PMTs, including hardware and installation, analysis of signal and noise of the PMTs, modelisation and fitting of the noise, and analysis of its dependency in other external phenomena.

This chapter will be the opportunity to present my experience on PMT hardware and my contribution in their installation in dark rooms, as an uncommon but essential work for the Hyper-Kamiokande project. Then, I will present the unexpected result of these measurements, to the point of threatening the continuation of PMT mass production. This motivated new measurements and further analysis of PMT dark noise, that I realized, which allowed me to bring the key arguments to pursue the mass production.

2.1 Introduction on Dark Noise

2.1.1 Definition and origins of dark noise

As presented above (see Section 1.5, the component used in Super-Kamiokande or Hyper-Kamiokande to acquire the signal is photo-multiplier tubes (PMT). They are designed to detect light with enough precision to detect single photons as "hits". Therefore, the expected behaviour of a PMT remaining in a completely dark room is to record no hit at all. However, we observe that PMTs in dark rooms do generate hits. This remaining "signal" is called dark noise.

As far as we know, dark noise has two main origins: glass scintillation and thermal electrons. In short terms:

- Glass scintillation describes the fact that the glass surrounding the photo-sensor can eventually emit some photons inside the gas without any external cause, that will then hit the photocathode and generate a signal.
- Thermal electrons are electrons that are present in the tube and will eventually hit the anode because of nonzero temperature.

These two noises and the methods used to analyse them will be further described in Section 3.3

2.1.2 Dark rate

The way we commonly use to characterize dark noise is the dark rate, which is the average frequency of these "fake hits". Of course, it doesn't encapsulate all the information about dark noise. For instance, it doesn't take into account the repartition of hits in time, but this will be discussed in Section 3.3.

The typical expected value for the dark rate in the last phase of Super-Kamiokande or in Hyper-Kamiokande is around 4kHz.

2.1.3 Hit detection in the raw PMT signal

In order to understand how this noise is evaluated and analysed, let's focus quickly on hit detection in the PMT signal. The raw signal of the PMT consists in a voltage for each time step. We can then draw a monitoring plot of PMT voltage over time, as shown in Figure 2.1. The orange curve shows the so called baseline, that is, the noisy flat curve observed when no hit is recorded. However, when a hit happens, the accumulation of charge in the anode causes a decrease in the measured voltage, which is characterized as a pic below the baseline, as shown on the blue curve.

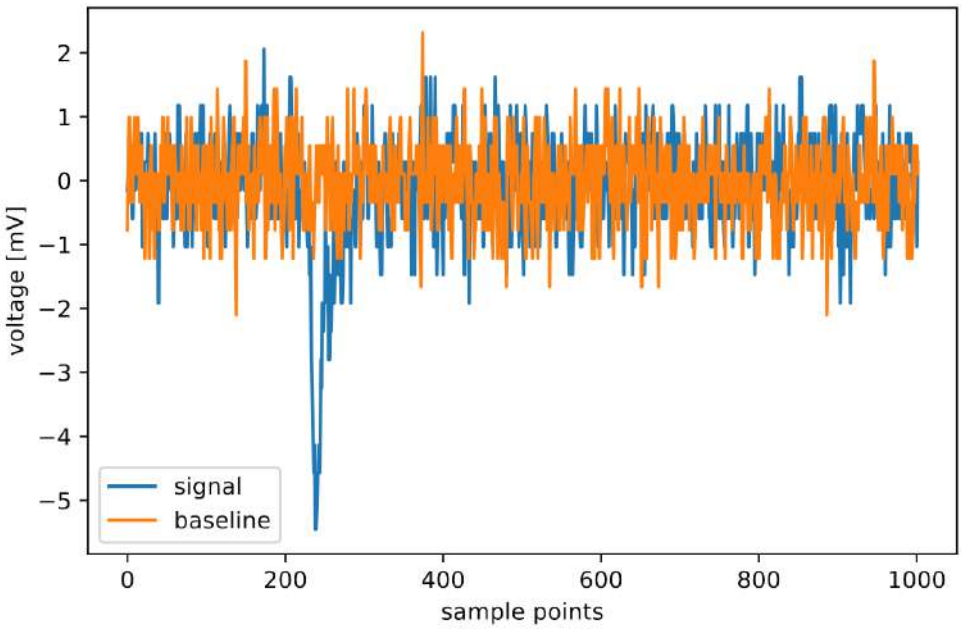

Figure 2.1: Two kinds of photomultiplier signals: baseline (orange) and signal (blue). A hit is detected as a pic below the baseline.

Then, if we want to count the number of hits in a certain period of time, we can draw an histogram of the values of that voltage. All the values around the baseline will form a component named the pedestal, which corresponds by definition to 0 photo-electrons (phe), whereas the values issued from the hits will form another component at 1 phe. Furthermore, if some pics in the voltage result from multiple hits happening at the same time, other components will result at multiple phe. This process is illustrated in Figure 2.2.

Once this histogram is built, we can simply count the number of hits by fitting the different components [3]. The dark rate can finally be obtained by dividing this number of hits by the length of the time window. This is the method I use in my study to evaluate the dark rate.

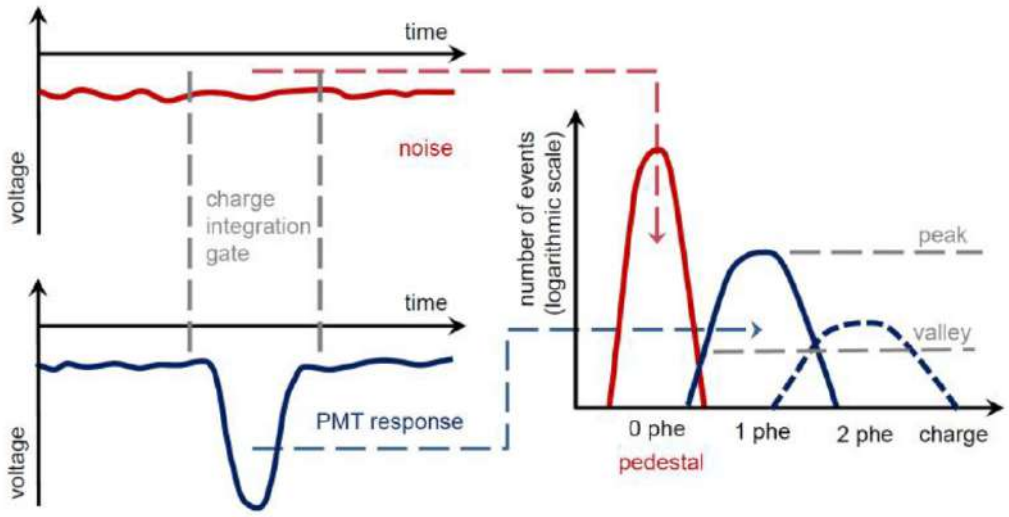

Figure 2.2: **Left:** PMT signal acquisition. Upper graph shows no signal, the lower graph shows a single photoelectron response. The area enclosed by the integration gate represents the deposited charge used to form the charge spectrum. **Right:** Qualitative single photoelectron spectrum splitted into its single components. [3]

2.2 Dark Rate measurements in Kamioka

2.2.1 Installation work

As an essential part of the work in the Hyper-Kamiokande collaboration, two weeks of my internship were dedicated to hardware work on PMTs in Kamioka, near the actual site of Super-Kamiokande and the construction site of Hyper-Kamiokande, that I could both visit.

The purpose of my work in Kamioka was to setup a new dark room and install one hundred PMTs in it, in order to start new measurements of dark rate. These measurements are essential to verify the well-functioning of the PMTs, in conditions close to the real conditions in Hyper-Kamiokande. To that extent, the same cabling system and data acquisition methods than in real conditions are used (see Section 1.5), and the geographic proximity allows to assume same magnetic field, radiation (without taking into account the shielding that will be applied after).

Some pictures of the installation work I realized are presented in Figure 2.3. This work essentially includes the following tasks:

- Delivery and storage of the new PMTs in the appropriate building in Kamioka town
- Building the slots on which the PMTs will be laid
- Bringing and setup the appropriate devices for high voltage and data acquisition near the dark room
- Building the high voltage boxes, that allow the connection of the PMTs to the high voltage generator
- Setup the cables in the dark room at the right positions, and connect them to the generator and devices responsible of the data acquisition
- Disposing the 100 PMTs in the dark room, and plugging them to the cables

Figure 2.3: Installation work in the new dark room in Kamioka.

2.2.2 Measurement results

As specified above (2.1.2), the expected value for the dark rate for Hyper-Kamiokande PMTs in about 4kHz, a value that is confirmed by the prior measurements made by Hamamatsu just after PMT construction. However, the analysis of the measurements conducted in Kamioka (described in 2.2.1) lead to a measured value of the dark rate of around 8kHz, which is far above what we can afford. Despite many checks, the measurement setup could not be blamed, which lead to consider this value as correct.

After some investigation, one external element was identified to explain this difference. Indeed, the radiation level is higher in Kamioka than for the prior measurements in Hamamatsu, which could explain this difference. If this is indeed the explanation, then the problem is solved, as the PMT will be shielded against radiation in real conditions. However, nothing allowed to affirm with certainty that this is the cause, and that the dark rate would be lower in real conditions. Therefore, it was decided to stop the PMT mass production until this problem is clearly identified, which is the task that fell to me.

2.3 Dark rate measurements in Kashiwa

2.3.1 New dark rate measurements in Kashiwa

In order to solved the problem exposed above (2.2.2), it was decided to conduct new measurements for a small group of 8 PMTs in Kashiwa (campus of Tokyo University, in the north of Tokyo). This place was rather convenient for this task, as a darkroom was already present there, and the radiation level is much lower than in Kamioka, which is the parameter we wanted to test.

Thus, I went to Kashiwa campus to contribute to receive and install these 8 PMTs in the dark room, and setup the data acquisition system. Given this dark room was small and not designed for large scale measurements, the usual data acquisition methods were unthinkable, as they are too expensive and take too much space. Instead, a full signal acquisition through oscilloscopes was setup. This method has of course many other flaws, such as storage issues and systematic errors coming from the difference with the usual setup. But for a small number of PMTs and a rather short period of time (3 months), storage could be managed, and the precision need was not high enough to take the systematics into account.

Among the eight chosen PMTs, four of them are from the *original design* and four of them are from the *improved design*, which results from ameliorations made to the PMTs after the beginning of the production. Furthermore, four of the PMTs (two original and two improved PMTs) are plugged to one oscilloscope, and the four other ones are plugged to another oscilloscope. These oscilloscopes are named *IPMU oscilloscope* and *KEIO oscilloscope* on the following figures.

2.3.2 Measurement results

In order to take measurements with the oscilloscopes in Kashiwa from the laboratory in Keio University (south of Tokyo), a connection had to be established with ssh procedures. A non negligible amount of work had to be spent on writing scripts to connect and send requests to the oscilloscopes periodically, and then collect the data and transfer it back to the servers in the University.

The acquisition was made every hour during the first week, and then twice a day. Each acquisition consists in full signal acquisition during 1 second. The signal is then treated to identify the number of hits in the time window (using the method described in Section 2.1.3), which allows to determine the dark rate. This is done for each of the eight PMTs, and the results can then be shown in a monitoring plot, see Figure 2.4.

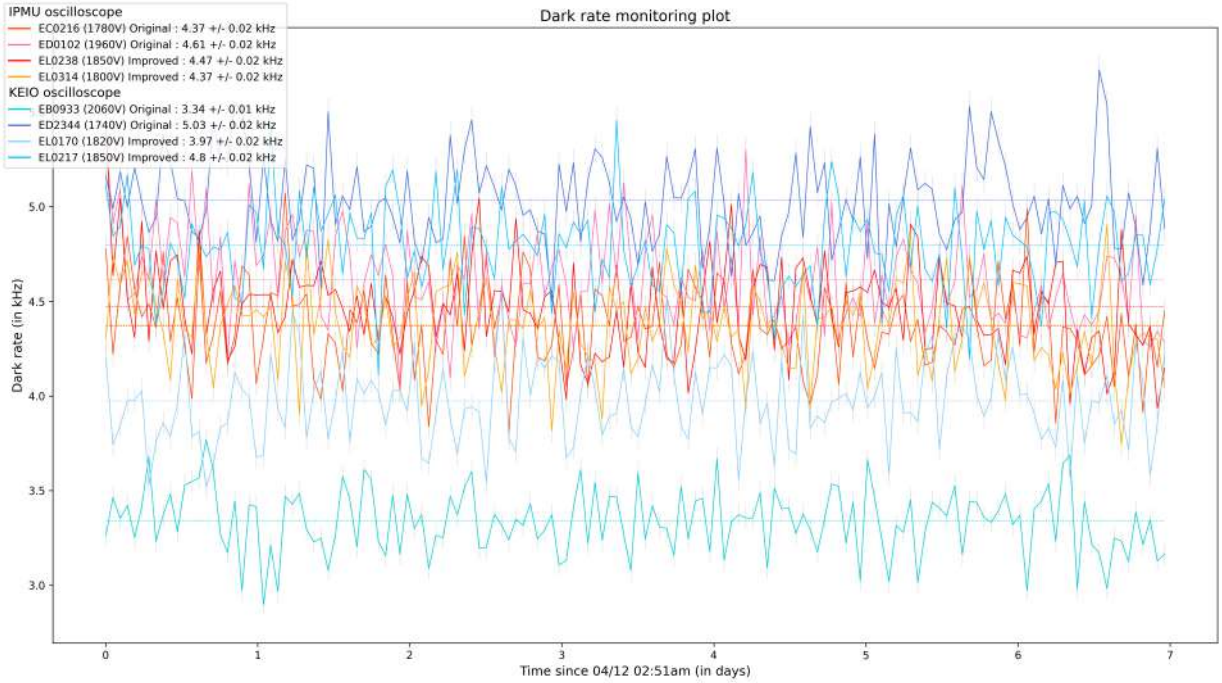

Figure 2.4: Monitoring plot of the dark rate during the first 7 days.

The fact that the 8 PMTs have different dark rates is expected and normal, as it is very difficult to control this property (as well as other properties such as quantum efficiency, cathode blue sensitivity, etc.), and the PMTs that present very bad performances after being tested in Hamamatsu are simply rejected. However, surprisingly, the observed variations in time (approximately 0.5kHz) are much higher than the statistical error, which can be evaluated as follows:

$$\sigma = \frac{\sqrt{N}}{T} = \sqrt{\frac{r}{T}} \approx 0.1kHz$$

where N is the number of hits during the time window, $T = 1$s is the length of the time wondow, and $r = \frac{N}{T}$ is the dark rate.

This is explained empirically by the presence of noise in the cabling with the oscilloscope, which biases the analysis of the signal and hence hit count.

The full results are presented in Figure 2.5. As the average dark rate in Kashiwa is 4.3kHz, these results are very comforting concerning the performances of the PMTs, and were a key argument in favor of restarting the mass production of PMTs.

	Serial	(HV)	Skb (µA/lmF)	Rate at Kamioka (after 6 days)	Rate at Kashiwa (after 6 days)	Rate at Kashiwa (after 45 days)
Original	EB0933	(2060V)	10.8	7.2	3.4	3.4
	ED2344	(1740V)	10.7	9.1	5	4.7
	EC0216	(1780V)	11.5	10.3	4.4	4.3
	ED0102	(1960V)	11.3	9	4.5	4.4
	Average of original PMTs			8.9	4.3	4.3
Improved	EL0170	(1820V)	10.5	8.2	4	4.1
	EL0217	(1850V)	11.1	7.8	4.7	4.7
	EL0238	(1850V)	11.3	10.6	4.4	4.4
	EL0314	(1800V)	10.9	8.5	4.3	4.3
	Average of improved PMTs			8.8	4.4	4.3
	Average of 8 PMTs			8.8 kHz	4.3 kHz	4.3 kHz

Figure 2.5: Measured dark rate in Kamioka and in Kashiwa for the 8 PMTs. HV is the High Voltage and Skb is the cathode blue sensitivity - no correlations were found between these parameters and dark rate.

Chapter 3

Dark rate dependency on temperature

After conducting a study on dark rate monitoring, which implied the displacement and setup of 8 PMTs in a different environment than their original one, it appeared that we could benefit from that to study other phenomena on PMTs. In particular, this environment appeared to be convenient to regulate temperature, and hence study the influence of temperature on dark rate. This study appeared to give interesting results, and lead me to make a presentation in Hyper-Kamiokande international collaboration meeting in June 2023.

3.1 Motivations

Knowing the dark rate dependency on temperature is very useful in order to predict the performances of the PMTs in real conditions based on their performances in benchmark. Indeed, as it is explained in Section 3.3, the dark rate varies with temperature. Furthermore, it is made up of two components which increase at $T \to 0$ and $T \to +\infty$, therefore there is a minimum for a finite temperature. It turns out that this minimum is usually around 14°C, which is precisely the temperature inside the tank of Hyper-Kamiokande.

However, the law that dictates the dependency on temperature depends on a set of parameters, that can vary with the type of PMTs and between the different PMTs themselves. Thus, studies are needed to determine these parameters and infer this law. Once the law is known, it becomes possible to deduce the performances of the PMTs in real conditions from their performances in benchmark with better precision.

Studies about temperature dependency had already been conducted before in Kamioka, but only on small ranges (around 14 ± 1°C), and with the problems inherent to the measurements in Kamioka (see Section 2.2.2). Therefore, this study is the first one on a large temperature range and in another place than Kamioka.

3.2 Experimental Setup

The physical setup remains the same as in the previous chapter 2.3.1: 8 PMTs (4 *original PMTS* and 4 *improved PMTS*) are installed in a dark room and plugged to two oscilloscopes, that can acquire the full signal. The dark room is equipped with thermometers that can monitor the temperature in real time, and the temperature inside the dark room can be set at any value between −5°C and 22°C.

In order to have measurements on all the range of temperature, the temperature has been set at 2°C for a small period of time, and then the cooling was stopped to let the room warm up to

22°C. This operation was done a second time, cooling down at −5°C this time, before letting the room warm up again. The temperature variations are shown in Figure 3.1, as well as the dark rate measurements during the same period.

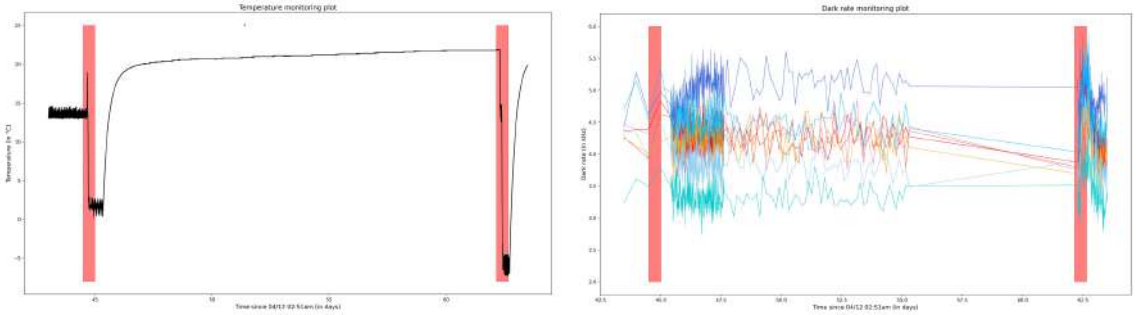

Figure 3.1: **Left:** Variations of temperature during the study on dark rate dependency on temperature. **Right:** Measurements taken during this study. the red rectangles indicate that the measurements in these areas were not taken into account, as the variation of temperature was too abrupt.

It is obvious on the temperature profile that the measurement points will not be equally distributed in the temperature range, and this is confirmed if we plot the dark rate as a function of temperature, as shown in Figure 3.2. One can also see that the huge variations of dark rate (±0.5kHz) remain unfortunately. But there is still a sufficient amount of points to study the temperature dependency, furthermore given a model that just needs to be fitted.

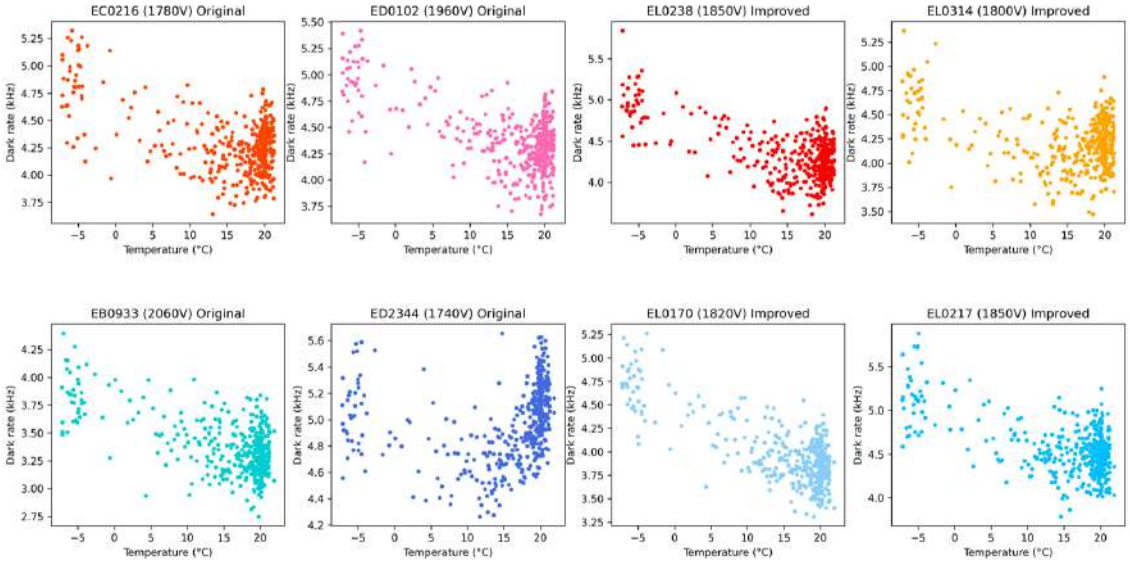

Figure 3.2: Dark rate dependency on temperature for the eight PMTs.

3.3 Scintillation and thermal noises

As we can see on Figure 3.2, the overall shape of the dark rate as function of temperature presents at least two components: one increasing at $T \to 0$ and one increasing at $T \to +\infty$. These two components can be explained and modeled by looking in details to the origins of dark rate, which are glass scintillation and thermal electrons.

3.3.1 Thermal noise

Due to nonzero temperature, thermal electrons are present in the photo-multiplier tubes and will eventually hit the anode. These hits are then recorded in the signal and contribute to the dark rate as "fake hits". Because of this purely random process, the thermal hits are statistically uniformly distributed in time. Therefore, the distribution of the time differences between two consecutive thermal hits follows an exponential distribution. This constitutes the green component on Figure 3.3, that is explained in section 3.3.3.

The dependency on temperature of the thermal noise can be modeled by the Richardson distribution, which is the following:

$$r_R(T) = AT^2 e^{-\frac{W}{kT}}$$

where W is the work function of the material, k is the Boltzmann constant and A is a scaling parameter.

3.3.2 Scintillation noise

Glass scintillation is a phenomenon that can occur due to the interaction between the glass surrounding the photo-sensor and the gas between the glass and the photocathode. This scintillation produces photons that will eventually hit the photocathode and produce hits in the PMT. The "fake hits" originated from glass scintillation are characterized by the fact that they are not uniformly distributed in time but grouped, as it is more likely that many photons are generated by the same glass scintillation event. This results in a distribution of time differences between consecutive scintillation hits that is different than an exponential distribution and more grouped around low values. This constitutes the red component on Figure 3.3, that is explained in section 3.3.3.

Scintillation noise dependency on temperature can be modelled empirically by an exponential law, as follows:

$$r_{nt}(T) = GA_c e^{-\frac{T}{T_r}}$$

where A_c is the area of the photocathode, G is a scaling parameter and T_r is a shape parameter.

3.3.3 Noise separation

As explained above, these two noises are distinguished by the distribution of time distributions between consecutive hits, which is exponential for thermal noise and grouped around 0 for scintillation noise. Figure 3.3 shows a plot of such distribution, where the exponential component is fitted on high time values and shown in green, and the scintillation component is deduced as the remaining component.

Unfortunately, for real data acquisition, that is done only during one second for each measurement, there are not enough hits to fit these components precisely on such plot. This is why we chose instead to apply cuts to separate these two components. Thus, Figure 3.3 shows that a cut at 150µs allows to extract a time range $[150; +\infty[$ on which thermal noise is dominant, whereas a cut at 20µs allows to extract a time range $[0; 20]$ on which scintillation noise is dominant. The partial components thus extracted are reasonably expected to represent the shape of dependency on temperature, which will allow a better evaluation of the shape parameters in $r_R(T)$ and $r_{nt}(T)$.

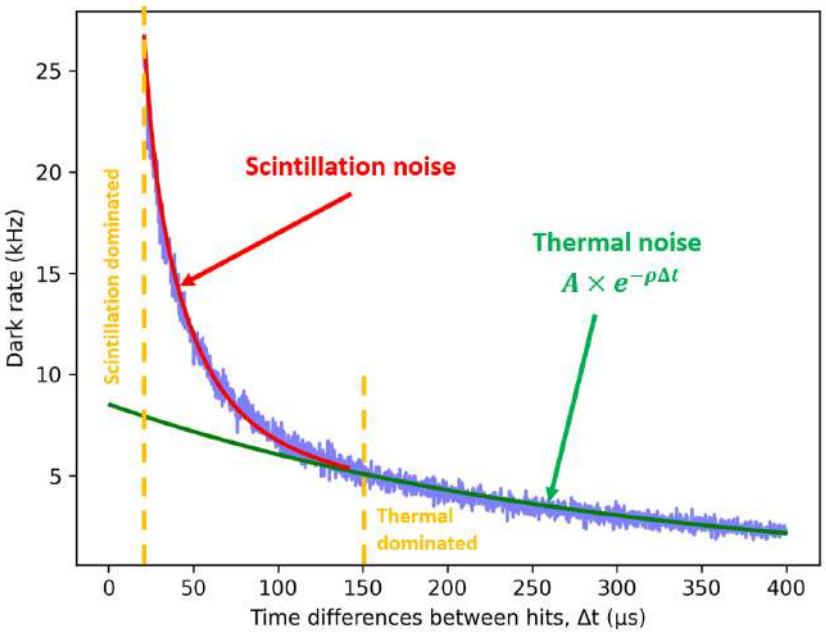

Figure 3.3: Distribution of time differences between consecutive hits of dark noise, and fitting of thermal (in green) and scintillation (in red) components. The orange dashed lines show the cuts that are applied to extract these two components.

3.4 Fitting the model

After establishing the model (3.3), we now have to fit this model on the data. The complete model reads as: $r(T) = r_{nt}(T) + r_R(T) = GA_c e^{-\frac{T}{T_r}} + AT^2 e^{-\frac{W}{kT}}$ with four parameters to fit: GA_c (the product is considered as one unique parameter), T_r, A and W.

Unfortunately, fitting the model directly does not work, as the data is not qualitative enough to fit four parameters with an acceptable precision. Most of the fitting algorithms, such as non-linear least squares, do not converge at all. Thus, more tricks are needed to perform these fit.

3.4.1 Normalization

First of all, most of the convergence problems can be solved by slightly changing the formula so that the parameters are in a controllable range. Therefore, the formula of $r(T)$ is modified as follows:

$$r(T) = GA_c e^{-\frac{T-T_0}{T_r}} + A\left(\frac{T}{T_0}\right)^2 e^{-\left(\frac{W}{T}-\frac{W}{T_0}\right)}$$

where T_0 is chosen as $T_0 = 15°\text{C}$ to be in the range of the data.

With such normalization, the scale parameters become easily controllable, as they should be equal to the dark rate at T_0, $r(T_0)$, which is measured. Thus, we can restrain the search of these parameters in the range $[0; 5]$ kHz.

Concerning the shape parameters, the work function W is known to be in the range $[0; 1]$ eV, and a quick look at the shape of the data show that a reasonable range for T_r is $[0; 1000]$ K.

3.4.2 Fitting the scintillation parameters

Even after normalizing the formula, a direct fit of these four parameters gives imprecise and even nonphysical values. However, we described earlier a method to separate scintillation and thermal components (see Section 3.3.3), which can allow better precision separately on scintillation and thermal parameters.

So, the cut at 20µs shown in Figure 3.3 allows to extract the scintillation part of the data, on which we can fit the normalized function $r_{nt}(T)$. The results are shown in Figure 3.4.

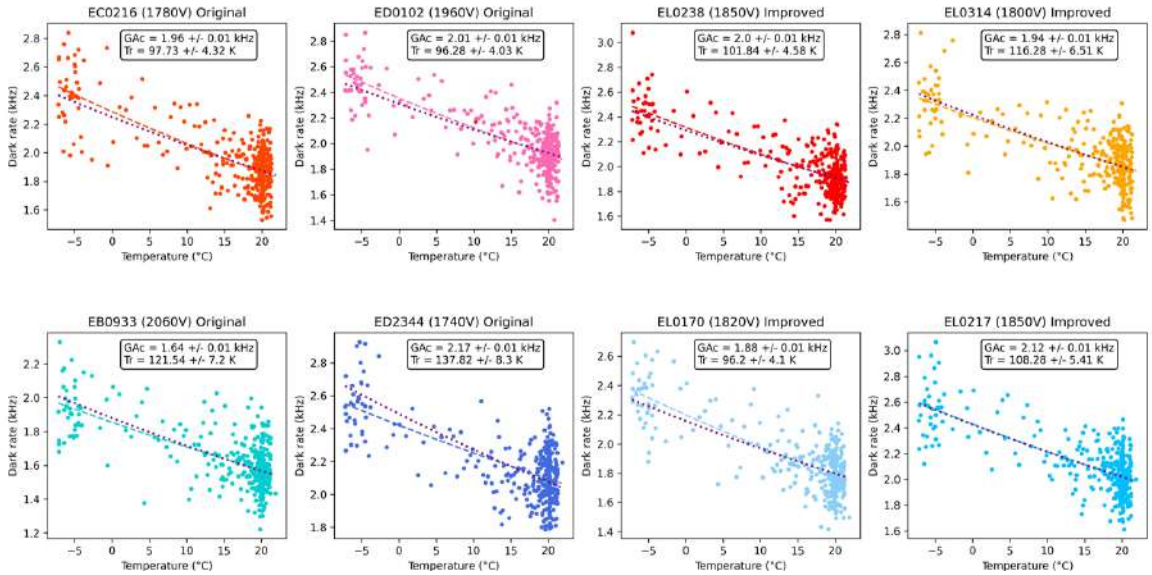

Figure 3.4: Scintillation part of the dark rate as a function of the temperature for the 8 PMTs. The dashed line is the fit by $r_{nt}(T)$ for each PMT separately, and the purple dotted line is the fit by $r_{nt}(T)$ with shared T_r parameter, taken as the average of the 8 T_r parameters. The GA_c parameter is kept different for each PMT.

Even if it is still not very precise, the errors on T_r are about 5%, which is acceptable, while the error on GA_c is very small (about 1%) because of the normalization.

In principle, the scintillation phenomenon is supposed to be the same for all the PMTs. The scale parameter, representing the amount of these hits happening, may not be the same for all PMTs, but the shape parameter T_r, intrinsic to the physical phenomenon is supposed to be the same. Therefore, for everything below, we keep one unique T_r parameter for all the PMTs, which is determined as the average on the 8 PMTs:

$$T_r = 109 \pm 14\text{K}$$

This comes of course with a bigger error, but it is more physically correct and expected to be more generalizable.

3.4.3 Fitting the thermal parameters

Fitting the thermal parameters appears to be slightly more difficult than expected. We can first expect to follow the same procedure as for the scintillation parameters, that is, fitting the function $r_R(T)$ on the thermal part of the data using the cut at 150µs highlighted in Figure 3.3. But, it is clearly visible on the data (see Figure 3.5) that the noise separation is imperfect and that some scintillation component remain even after the cut.

One first approach that is considered is fitting the $r_R(T)$ function only on the high temperatures range $[15; 22]$ °C. This is done in Figure 3.5. However, the errors for W are particularly high with this method (usually around 15%, up to 100% and above), and the values obtained for W, which are $W \in [0; 0.15]$ eV, are rather nonphysical.

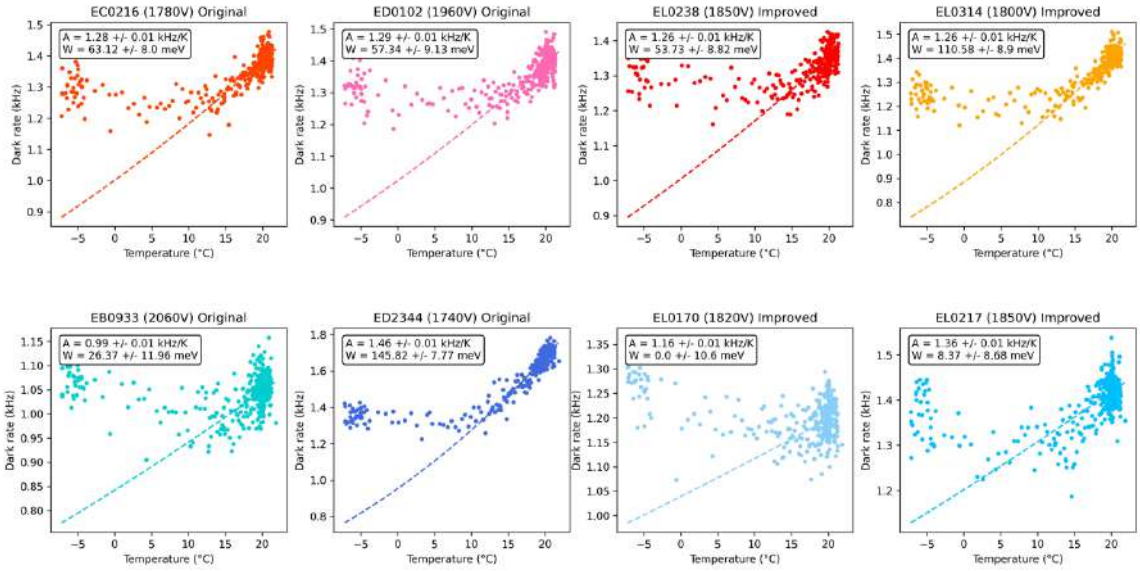

Figure 3.5: Thermal part of the dark rate as a function of the temperature for the 8 PMTs. The dashed line is the fit by $r_R(T)$ for each PMT separately, only in the range $[15; 22]$ °C. The range $[-5; 15]$ °C clearly shows that a scintillation component remains.

Another approach is to include the scintillation function $r_{nt}(T)$ in the fit also, that is, fitting with the whole function $r(T)$. This allows to perform the fit on the whole range and to get rid of the remaining scintillation part at the same time. For the scintillation part, the T_r parameter evaluated in Section 3.4.2 is used. The results of this method are presented in Figure 3.6. Note that only the fitting method is different, but the data is exactly the same as in Figure 3.5.

With this method, the errors on W are still very high, but the values are closer to the expected values for work functions. Therefore, we use this method to evaluate the W parameter.

This time, the parameters are kept different for each PMTs, as thermal electrons noise is not expected to be the same for all PMTs. In particular, the work function W can differ between the PMTs and is difficult to control in the confection. Thus, we could determine a range for the W parameters, which is the following:

$$W \in [0.1; 0.7] \text{ eV}$$

The W parameters evaluated here for each PMT will now be kept fixed for the following.

3.4.4 Scaling the two components

Now that we know the shape of the scintillation and the thermal components (that is the T_r and the W parameters), all that's left is to determine the weights, or scale, of these components in the whole data (without cut), including both full scintillation and full thermal components. This is done simply by fitting the $r(T) = r_{nt}(T) + r_R(T)$ function on the whole data, while keeping T_r and W fixed. The results are presented in Figure 3.7.

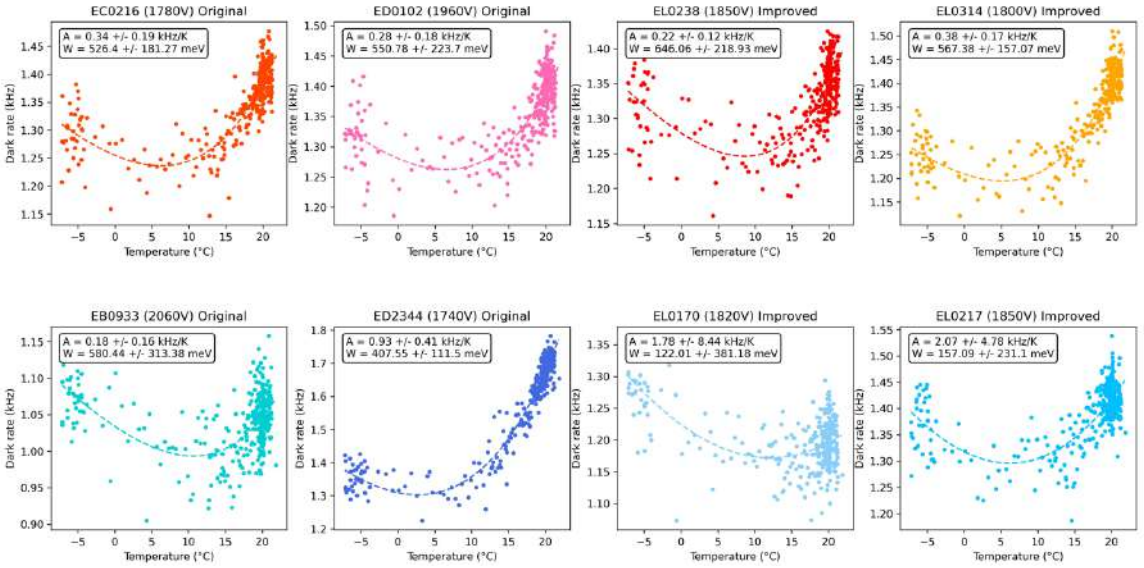

Figure 3.6: Thermal part of the dark rate as a function of the temperature for the 8 PMTs. The dashed line is the fit by $r_{nt}(T) + r_R(T)$ for each PMT separately. The T_r parameter evaluated in Section 3.4.2 is used, while all the other parameters are optimized to fit the data.

This time, given we are fitting the scale of the two components at the same time, the error on the GA_c and A parameters are very high (around 20% for GA_c and more that 100% for A). Even though, it still allows to establish ranges for the values of these parameters, that could be precised in the future with other studies. The ranges obtained are the following:

$$GA_c \in [3.2; 4.2] \text{ kHz}$$

$$A \in [0.2; 1.8] \text{ kHz}$$

3.5 Predictions of the model

Although the purpose of this study was to establish the model with adequate ranges for the parameters based on the available data, we can show preliminary results that the model implies. These results are summarized in Figure 3.8. T_{min} is the temperature at which the dark rate is minimal, while $r(T_{min})$ is the value of this minimum. The particularly interesting values are the following differences:

- $r(14°\text{C}) - r(T_{min})$ indicates the additional noise we get by working at 14°C in Hyper-Kamiokande instead of the optimal temperature T_{min}. This additional noise is 0.08 ± 0.13kHz in average, which is low enough to allow not making modifications of the PMT design or the temperature of the tank.
- $r(25°\text{C}) - r(14°\text{C})$ allows to predict the dark rate in the tank of Hyper-Kamiokande based on the measurements at Hamamatsu (which are made at 25°C). This difference is 0.14 ± 0.37kHz.

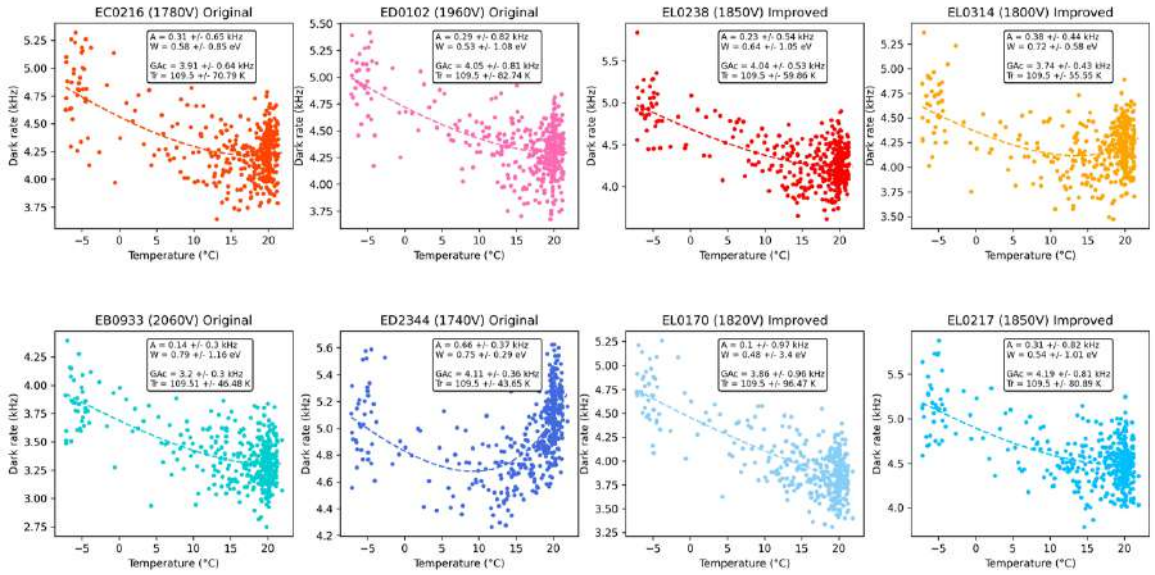

Figure 3.7: Dark rate as a function of the temperature for the 8 PMTs. The dashed line is the fit by $r_{nt}(T) + r_R(T)$ for each PMT separately. The T_r and W parameters evaluated in Sections 3.4.2 and 3.4.3 respectively are used, while all the scale parameters GA_c and A are optimized to fit the data.

	Serial	(HV)	Skb (µA/lmF)	Tmin (°C)	r(Tmin) (kHz)	r(14°C) - r(Tmin) (kHz)	r(-5°C) - r(Tmin) (kHz)	r(25°C) - r(14°C) (kHz)
Original	EB0933	(2060V)	10.8	20.0	3.3	0.05	0.55	0.00
	ED2344	(1740V)	10.7	9.2	4.7	0.06	0.32	0.96
	EC0216	(1780V)	11.5	17.9	4.2	0.02	0.53	0.07
	ED0102	(1960V)	11.3	20.7	4.3	0.06	0.61	-0.03
	Average of original PMTs			17.0	4.1	0.05	0.50	0.25
Improved	EL0170	(1820V)	10.5	37.4	3.7	0.39	1.06	-0.26
	EL0217	(1850V)	11.1	19.6	4.5	0.04	0.61	0.01
	EL0238	(1850V)	11.3	20.3	4.2	0.00	0.41	0.38
	EL0314	(1800V)	10.9	13.4	4.1	0.05	0.55	0.00
	Average of improved PMTs			22.7	4.1	0.12	0.66	0.03
	Average of 8 PMTs			19.8 ± 8.2	4.1 ± 0.4	0.08 ± 0.13	0.58 ± 0.22	0.14 ± 0.37

Figure 3.8: Predictions of the model for some specific values. T_{min} is the value at which the dark rate $r(\cdot)$ is minimal. 14°C is the temperature inside the tank of Hyper-Kamiokande and 25°C is the temperature for the test measurements at Hamamatsu.

Although they are not very precise, these values are the first ones for these parameters, and they allow to establish orders of magnitude and tendencies. Further studies may involve different measurement setup and have more precise measurements, leading to a better estimation of the parameters of the model. Also, whereas the scintillation component of the noise is quite well fitted, we seriously lack measurement at higher temperature to have fit precisely the thermal component of the noise. As the thermal component is the preponderant one between 14°C and 25°C, it is the most important one in the model, therefore further studies should focus on getting measurements at higher temperatures (ideally up to 30°C).

Chapter 4

Auxiliary work on neutron tagging analysis

Whereas my main work during this internship was about PMTs and dark noise, I was also assigned to a secondary work in parallel of PMT studies, which is a data analysis study for neutron tagging using machine learning. Given the time I could dedicate to this study, and the many problems that occured and that I figured out during the investigations, the purpose was not to directly have interesting results, but rather to setup a preliminary work in order to give it to another student who will continue this research. Therefore, this is mainly a work of documentation and reproducing previous studies in an easy-to-use environment, so that further investigations and improvements could be led by another student afterwards.

As a second feature that emerged from this preliminary study, I could also identify many key points that make such a study difficult to be performed without some specific conditions. Mainly, I figured out that the state-of-the-art open-source simulation tool for WCDs at high energy is actually quite bad at low energy, so that only the internal tools of SK collaboration could be used. Similarly, Gadolinium is a very central feature of neutron capture in Super-Kamiokande and Hyper-Kamiokande, but its simulation is currently handled very bad, which makes machine learning methods trainable only for hydrogen neutron capture. These key points that were highlighted in this study will hopefully allow a better preparation for the upcoming studies held by my laboratory in this field.

4.1 Introduction on Neutron Capture Concerns

Neutron Tagging is one of the most important topics in low-energy neutrino research. Indeed, being able to detect neutron captures in Super-Kamiokande or Hyper-Kamiokande helps discriminating neutrino and anti-neutrino events, which then leads to the estimation of the CP violation phase δ_{CP} in the leptonic sector.

As explained in section 1.3, the main interaction process for neutrinos at low energy is through charged current, and specifically inverse beta decay (IBD). There are two IBD processes, a neutrino induced one, and an anti-neutrino induced one, whose equations are the following:

$$\begin{cases} \bar{\nu}_l + p \rightarrow l^+ + n \\ \nu_l + n \rightarrow l^- + p \end{cases}$$

The outgoing charged leptons or anti-leptons are indistinguishable (for a same flavour), as they have the same momentum and energy distributions, and produce exactly the same Cherenkov

rings. However, the outgoing nucleus (proton or neutron) will have different behaviours. Whereas protons will simply thermalise and produce no signal, neutrons will be captured by another atom after thermalisation, and this capture will produce gamma rays that can be detected. A schematic representation of a neutron capture event is shown in Figure 4.1.

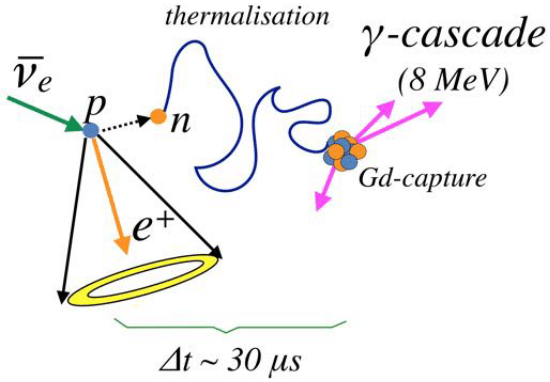

Figure 4.1: Schematic representation of a neutron capture event by a gadolinium atom. Image originated from [7]

The nature of the emitted gamma rays after the neutron capture depends on the atom the capture is made by. For hydrogen atom, the average time between the primary vertex and the neutron capture is 204 µs, and only one gamma ray is emitted at 2.2 MeV. However, with gadolinium doping, the average time before capture by a gadolinium atom is only $20\mu s$, and the multiple emitted gamma rays have a total energy of about $8MeV$. These properties motivated the insertion of gadolinium inside the water tank, which consequently improved neutron tagging performances.

4.2 Motivations for this study

While the usual methods for neutron tagging, and the most performant ones, work on various reconstructed parameters, some techniques begin to be developed to deal with the raw information of the PMT hits. Given that this information is very sparse and difficult to extract from noise, most of such techniques focus on machine learning. However, in 2023, these techniques cannot perform better than other existing methods yet.

The overall purpose of this study is therefore to investigate some techniques using the raw information of recorded PMT hits to perform neutron tagging task. Reproducing the work made by other researchers is a necessary step, as well as exploring some small deviations of it, everything being developped in an understandable and user-friendly way so that it can be used as a ground base for further studies.

Another interesting point that can be explored is the preselection that is held before the analysis. Current methods, even those working directly on raw data, are always performed after a preselection based on thresholding the number of hits in given time windows. However, no research study has shown interesting results yet about removing this preselection to include it in the machine learning process. While this could not be explored in details in this study, it is left for further investigations.

4.3 Data Simulation

4.3.1 Simulation tools

In order to develop and train machine learning methods for neutron tagging, we need a sufficient amount of data of neutron capture events in the water tank. Data simulation is absolutely necessary for machine learning methods, because it allows to have labeled data (that is, events for which we know exactly if they contain a neutron capture or not), but this raises the issue of the quality and the fidelity of this simulation. Indeed, the performances of the model on real data will highly depend on the quality of the data it is trained on.

Despite this not being the first thing we think about, this issue is actually a big problem for this kind of studies. For this work, we use the opensource tool WCSim [10], which allows to simulate particles propagation and interactions in water, as well as the induced signal and noise of the PMTs for a given Water Cherenkov Detector architecture. This tool is widely used for high energy studies for WCDs, which led us to think it would be appropriate for our study. However, it appeared that it is actually far less faithful for low energy events. The community of physicists working on low energy being much smaller, it took us time to realize this problem.

Currently, better tools exist especially for Super-Kamiokande, such as SKDetSim or SKG4, but Super-Kamiokande Collaboration membership is needed to access these tools, therefore they cannot be used in this study. Another source that makes simulated data unrealistic is the noise. Whereas real noise is composed of many sources (including muon spallation, afterpulses, radon, etc.), WCSim can only simulate PMT dark noise, which leads to incomplete and thus unrealistic noise. Consequently, the results of this study must be understood only as preliminary results, but not as directly applicable to real data. A full comparison between WCSim and SKDetSim can be found in [2].

Anyway, after experimenting myself and talking to experts in the subject, I came to identify the current consensus about these tools:

- A same model gives less accidental coincidences on SKDetSim data than on WCSim data (for the same signal efficiency), with a reduction factor that can reach 10.
- Replacing simulated noise by real noise data from SK ("dummy triggers") also improves the efficiency of the models consistently.

4.3.2 Simulated data for this study

In order to be able to test the models quickly, first "simple" datasets have been generated. The purpose being to discriminate between neutron capture events and noise events, two types of events have been generated:

- 100000 events of 200ns of 2.2 MeV gamma rays (with vertex inside the so called fidutial volume, that is, 2m away from all the borders of the internal tank), superposed with simulated dark noise at 4.2 kHz.
- 100000 events of 200ns of simulated dark noise at 4.2 kHz.

A model can then be trained to classify these two types of events, which can give a first indication of the performances of the model.

However, the data this kind of models are usually trained on are different. When analysing real SK data, the primary electron or positron event generates a trigger, and all the hits during a large time window of 535 µs are recorded after this. The search for neutron capture event is then performed on this long sequence. In order to reproduce that, we usually take sequences of about 500 µs of dummy trigger, and then randomly add simulated 2.2 MeV gamma rays inside it. The model is therefore charged to find the times when there is a neutron capture in these sequences. Figure 4.2 shows the usual setup for the simulation of neutron capture events.

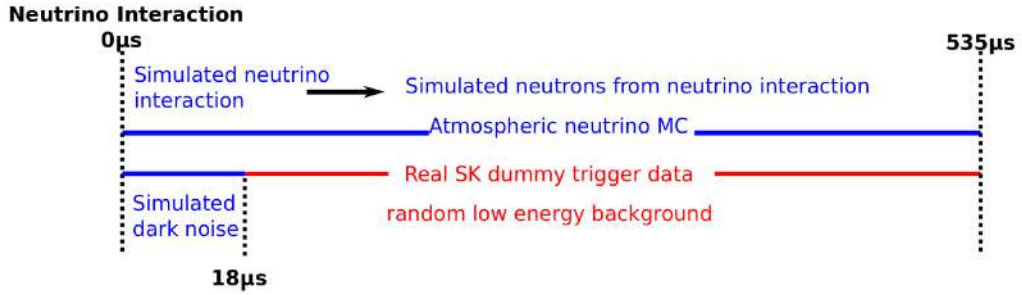

Figure 4.2: Construction of neutron MC, issued from [5]. After $18\mu s$ dummy trigger data is convoluted with simulated neutrons produced by an atmospheric neutrino interaction.

Unfortunately, given the time and resources dedicated to this study, this type of data could not be generated and analysed properly.

4.4 Data analysis with graph neural networks

Graph neural networks (GNNs) are a class of machine learning models, which is very generic and adaptable for different data formats. They are particularly convenient for the analysis of Super-Kamiokande of Hyper-Kamiokande data, as the data (a collection of hits on a cylinder in which we want to identify rings) has a very unusual topology, and is not well fitted for usual methods. However, GNNs are less powerful and less explored by the community than other specific architectures, which makes them difficult to take in charge and exploit. Nowadays, they are nearly the only machine learning architecture used for raw WCD data analysis at low-energy.

More explanations about GNNs and the way they are used for WCD data analysis are given in Appendix A. An illustration of a GNN used for vertex reconstruction from another study is given in Figure 4.3

The way GNNs are used for such analysis is usually the following:

- A preselection phase is performed, consisting in selecting the time windows which are likely to contain an identifiable neutron capture event. This usually consists in a treshold on the number of hits in a given window (e.g. $N_{10} \geq 7$, N_{10} being the number of hits within a 10µs window).
- Within the preselected windows, a graph is constructed. The nodes of the graph are the hits themselves (containing the position, timing and charge information), while the edges are usually computed with a clustering algorithm such as k nearest neighbours, and eventually associated with a weight depending on a certain form of distance between the hits. Many graph architectures exist, but none really emerged as a consensus.
- Once the graph is built, the GNN model can be executed on it. Many architectures also exist for the model itself, but they all share the same global shape.

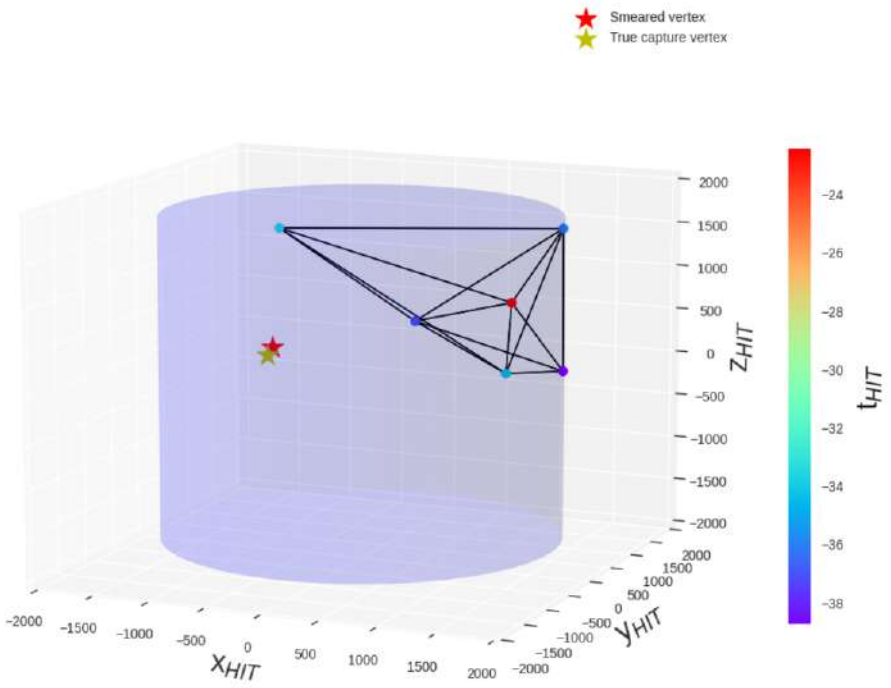

Figure 4.3: Illustration of a GNN used for vertex reconstruction at low energy in Super-Kamiokande. Image issued from [6]

4.5 Model evaluation in neutron tagging

In usual neutron tagging tasks, two metrics are important to evaluate a model: the efficiency, and the number of accidental coincidences per event.

- The efficiency is the proportion of real neutron capture events that are actually identified as neutron capture events by the model.
- The number of accidental coincidences per event is the number of noise windows that are said to contain a neutron capture by the model (while they do not) for each neutrino event.

Thus, when one creates a model, the objective is to maximize the efficiency while keeping the number of accidental coincidences per event low enough at the same time. Usually, for machine learning models, the model will compute a score for an input (here, for a time window of data), which is supposed to represent the likelihood of containing a neutron capture or not. Then, we can fix a threshold on this score, saying all the scores above the threshold mean we consider there is actually a neutron capture, and vice-versa. The metrics of efficiency and accidental coincidences per event then depend on this threshold, which we can fix in order to force the number of accidental coincidences per event to be low enough. Figure 4.5 for example shows curves of accidental coincidences per event as a function of the efficiency (for a moving threshold), called ROC curve.

Furthermore, as explained in Section 4.4 the central machine learning model (in our case, the GNN), is usually preceded by a preselection phase (see Section 4.4). This preselection phase itself can be associated with an efficiency and a number of preselected backgrounds per event, which are taken into account in the global metrics of the model.

Because of the way my data was simulated (see Section 4.3.2), the preselection cannot be performed exactly the same way than in real conditions, but we can still compute an efficiency and a background/event that are relevant. The efficiency of the preselection in my case is defined similarly as the proportion of 200ns neutron capture events that are actually preselected, and the number of backgrounds per event is defined as the proportion of 200ns noise windows that are preselected, multiplied by 2500 to take into account the fact that studies on real data search the neutron capture in 500µs windows with a 200ns sliding window.

4.6 Establishing the impact of the training context

While the study initially focused on reproducing existing methods and improving them, I quickly realized that the results I obtained were far worse than expected. As explained in Section 4.4, this is essentially due to the quality of the simulated data and noise. Therefore, I decided to add a new goal to this study, which is establishing a comparison between the performances of a given model in two different training contexts: the canonical one with SKDetSim data and Dummy Trigger noise, and the one used by non-members of the collaboration with WCSim data and noise. Such comparison will hopefully allow to establish more accurate reference performances for further studies using WCSim. Indeed, a model trained with WCSim could be compared to this reference model thanks to this "translation of performances". However, whether this comparison reflects the actual relative performances of the models on real data is still unclear.

The model used for comparison is one made by Antoine Beauchêne (LLR), whose results were presented at last Super-Kamiokande Collaboration Meeting (in June 2023).

- This model is initially trained on SKDetSim data with dummy trigger noise. The preselection used has an efficiency of 1.07 (with 96% distincts events extracted, as one neutron capture event can trigger the preselection algorithm more than once), and 1200 backgrounds/event. The results of the model trained in this setting are presented in Figure 4.5.
- I retrained this model with WCSim data and WCSim dark noise (at 4.2kHz). The preselection used here has similar results: an efficiency of 91% and 1150 backgrounds/event. The results of the model trained in this setting are presented in Figure 4.5.

As one can see, the results are very different. In particular, we retrieve the orders of magnitude mentioned above in Section 4.3.1, concerning the loss of performance between the two settings. For a given number of accidental coincidences per event, say 0.02 (a usual chosen threshold for this kind of tasks, see [1]), the efficiency is 30% in canonical setting, and 1% in our setting. We thus observe a reduction factor of roughly 30 for the efficiency in this region. For higher number of accidental coincidences per event, for instance 1, we observe an efficiency of 60% in the canonical setting and 10% in our setting, that is, a factor of 6.

Establishing this comparison was particularly useful for my study, as it allowed me to understand the origin of the low performances of my models. Indeed, I could reproduce similar performances to these ones with different GNN models (though all based on the same concept, with small variations in the architecture of the model or the clustering algorithms for graph construction), and this comparison helps comparing them to the state-of-the-art. Unfortunately, given their performances and the time I spent to understand that and build this comparison study, these models are not worth being presented in details in this report.

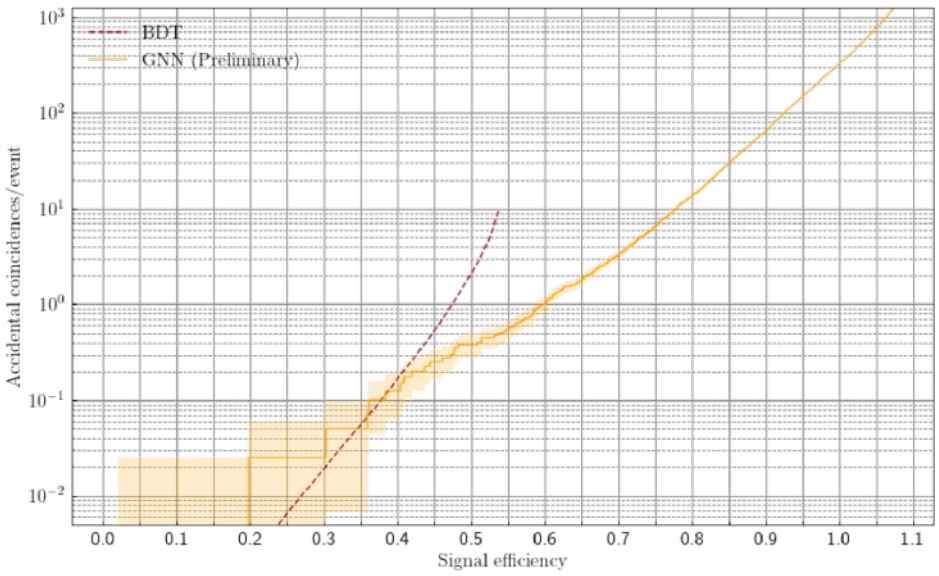

Figure 4.4: ROC curve of the model made by Antoine Beauchêne (LLR) trained on SKDetSim data with dummy trigger noise (canonical setting).

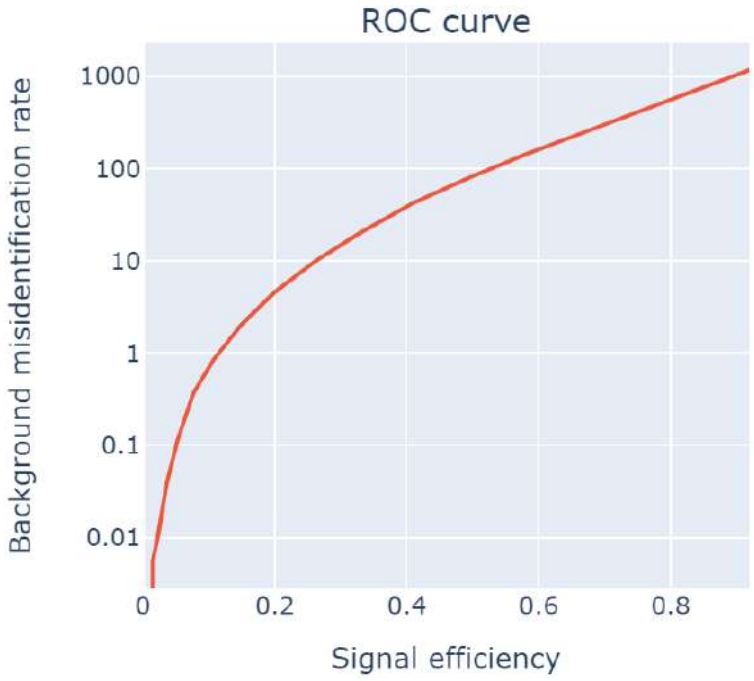

Figure 4.5: ROC curve of the model made by Antoine Beauchêne (LLR) trained on WCSim data with simulated dark noise.

Conclusion

Only armed with the knowledge I learned in master lectures, I had to dive head first into the rich and unknown world of experimental particle physics, beginning with the gigantic Hyper-Kamiokande experiment. Retrospectively, I can say that my appetite for discovery and understanding of this new world is satisfied in a better way that I even imagined.

First, the devotion of my supervisor, Nishimura-san, allowed me to access many opportunities of discovery into the work of the collaboration, which I seized as much as possible. I managed not only to see, but also to contribute to the work on many aspects at different levels of the experiment, from hardware and electronics near the detector itself to the abstract analysis of invisible signals at low energy, passing by the analysis of the PMT signal and behaviour.

Not all my projects evolved as expected, as one can understand by reading my report on neutron tagging analysis, but the adaptation and redesigns of the project that followed were not less interesting, as they are part of the experimental process. Moreover, knowing that my work will be pursued in the future by some other student in the laboratory is very satisfying. However, I am also proud of the success of my studies on PMT dark rate, which led first to political decisions at the scale of the collaboration, that is the restart of the PMT mass production, and second to a presentation at the Hyper-Kamiokande international collaboration meeting. I am now filled with the feeling of having contributed usefully to an enterprise beyond myself.

This internship was a key step in my studies in High Energy Physics, as it was for me the discovery of the experimental world. While my master course is half its way, I am now considering doing my PhD in experimental physics, because of this global context of collaboration that I like very much. However, I also lack knowledge of the theoretical world, and I plan to dedicate all my efforts in discovering it during my next semester at ETH Zurich. Hopefully, this will allow me to be well armed to pave my path in the world of research.

Bibliography

[1] K Abe et al. "Neutron tagging following atmospheric neutrino events in a water Cherenkov detector". In: *Journal of Instrumentation* 17.10 (2022), P10029.

[2] Farzan Beroz. "Water Cherenkov Simulation Tuning and Comparison". In: *APS Southeastern Section Meeting Abstracts*. Vol. 77. 2010, DA–012.

[3] Anna Eimer. "Measurement of PMT dark rates for the IceCube mDOM". In: (2021).

[4] J. A. Formaggio and G. P. Zeller. "From eV to EeV: Neutrino cross sections across energy scales". In: *Rev. Mod. Phys.* 84 (3 Sept. 2012), pp. 1307–1341. DOI: 10.1103/RevModPhys.84.1307. URL: https://link.aps.org/doi/10.1103/RevModPhys.84.1307.

[5] Tristan-James Irvine. "Development of neutron-tagging techniques and application to atmospheric neutrino oscillation analysis in Super-Kamiokande". PhD thesis. University of Tokyo (), 2014.

[6] *Low-energy reconstruction techniques at Super-Kamiokande, IRN Neutrino 2021 : https://indico.in2p3.fr/event/24095/contributions/95557/attachments/64852/90113/sklowe_reco.pdf.*

[7] Pablo Fernández Menéndez. *Neutrino Physics in Present and Future Kamioka Water-Čerenkov Detectors with Neutron Tagging*. Springer, 2018.

[8] Matthew Stubbs. "Using Machine Learning to Improve Neutron Tagging Efficiency in Water Cherenkov Detectors". PhD thesis. University of Winnipeg, 2021.

[9] Yue Wang et al. "Dynamic graph cnn for learning on point clouds". In: *ACM Transactions on Graphics (tog)* 38.5 (2019), pp. 1–12.

[10] *WCSim git repository : https://github.com/WCSim/WCSim.*

[11] Wikipedia. *Cherenkov radiation*. URL: https://en.wikipedia.org/wiki/Cherenkov_radiation.

APPENDIX

A Graph neural networks for WCDs

A.1 Concept of graph neural networks

The main tool that we are using to perform data analysis at low-energy in WCDs is Graph Neural Networks, as they can have similar advantages as Convolutional Neural Networks (CNNs), but also allow a greater flexibility. Indeed, Convolutional Neural Networks are based on convolving a grid-shaped data (such as a sequence or an image, which contains a vector of data, called features, at each cell of the grid) with a kernel (see Figure 6). However, Super-K or Hyper-K data have the geometry of a cylinder, and are therefore very unsuitable for CNNs. Furthermore, for low energy events, the data is very sparse (there are very few hits, which are distanced from one another), which make it even less suitable for CNNs.

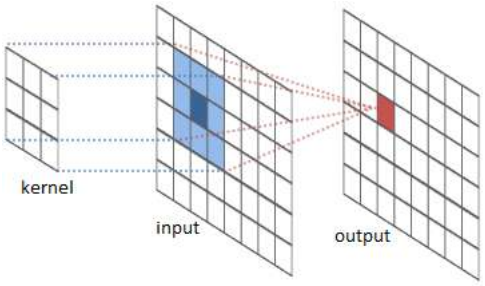

Figure 6: Illustration of a Convolutional Layer in a Neural Network. The kernel moves on the input grid, selecting successively a small part of the data and computing the associated output by a linear transformation of the local features. A new output grid is thus created.

On the other hand, graph neural networks (GNN) allow to manage these two problems. To the purpose of this study, deep knowledge of Graph Neural Networks is not needed, and we will only explain some key ideas. Instead of organizing the data as a grid, we can more generally organize it as a (eventually weighted and/or oriented) graph (the grid being a specific type of graph). As for the grid, the nodes of the graph contain the features, but the edges can also carry information. Then, the so called Graph Convolutional Layers allow to transform such graph into a new one, thanks to local information aggregation at a node from its neighbours, or message passing through the edges (see Figure 7).

The way we use Graph Neural Networks for WCDs is typically by making a node for each PMT hit in the considered event (or time window), assigning it some features (typically the position (x, y, z) of the PMT, the charge q of the hit and the time t of the hit), and linking the nodes according to some clustering algorithm (for example k-nearest neighbours). Further details about the theory of Graph Neural Networks and the way they are used for neutron tagging in WCDs are given in [8].

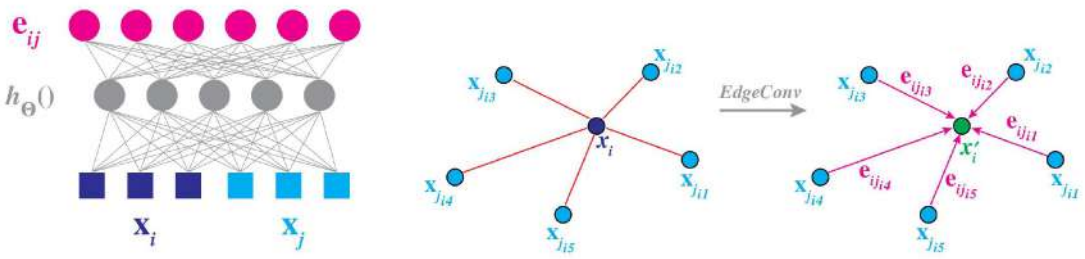

Figure 7: The Edge Convolution operation is shown for a pair of nodes x_i and x_j. The node feature vectors are passed through a fully connected layer $h_\Theta()$ with learnable weights Θ to calculate a set of edge features e_{ij} between the node pair. All nodes then update their vector representations by aggregating these learned edge features. In this example, the new representation of x_i, x_i' is calculated by aggregating the set of learned edge features $e_{ij_{i1}}, ..., e_{ij_{i5}}$. Figure retrieved from [9].

A.2 Graph construction

An essential step for applying GNN models to WCD data is to transform the raw data into a graph. The hits recorded in a given time window are the nodes of the graph, whereas there are multiple ways to select the edges. Usually, a clustering algorithm such as k nearest neighbours in the hit space (containing position, time and charge data) is used. But it is also possible to take only space or time distance into account, or compute some weights first (typically the inverse distance between the hits) and keep the edges with the highest weights. None of these methods emerged as a consensus, and no significant differences are observed.

A.3 Usual models

The architecture of the models developed in such study is the following:

- **Four graph convolutional layers.** The size of these layers, that is the number of features per node of the graph at the output of each layer, did not have big influence on the results, so it was typically chosen to be $5 \to 16 \to 32 \to 64 \to 128$ (the initial 5 corresponding to (x, y, z, t, q), the position, time and charge of the hits). However, the depth of the network, that is the number of layers, had significant effect on the performances of the model up to four layers.

- **One mean pooling layer.** This layer consists in aggregating the information of all the nodes of the graph by taking the average. Therefore, it takes as input a graph with 128 features per node (as it is the output of the last graph convolutional layer), and gives as output only one vector of dimension 128, which is the average of all the feature vectors (of dimension 128 each) of the nodes.

- **Two fully connected layers.** These layers simply transform a vector into another vector (see Figure 8), by applying a linear function followed by elementwise nonlinear functions (typically the ReLU function, see Figure 8). The sizes of these layers are typically chosen to be $128 \to 32 \to 1$. The final output is thus a number, that is the score used to discriminate between the two types of events (noise or $2.2MeV$ gamma ray).

The training process for this model is the very usual one for classification task. The binary cross entropy loss function is used to optimize the model :

$$\mathcal{L} = y \log(\tilde{y}) + (1 - y) \log(1 - \tilde{y})$$

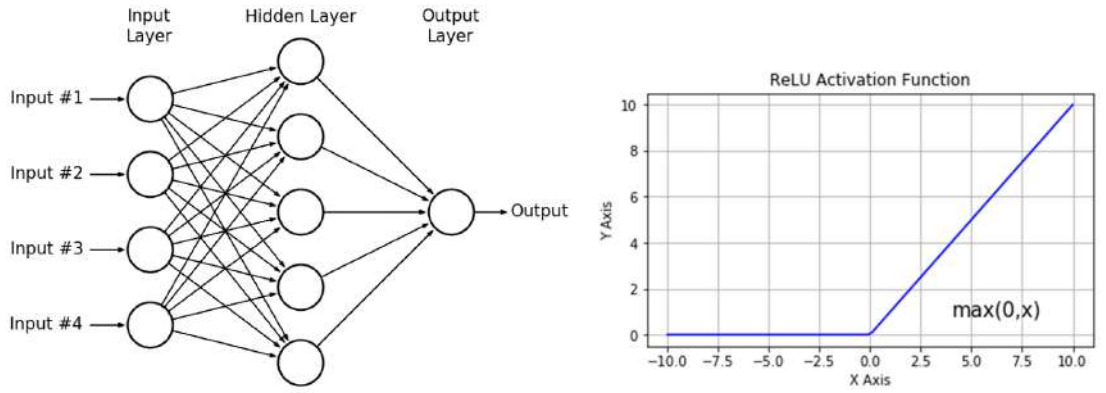

Figure 8: **Left:** Schematic representation of fully connected layers, consisting in linear functions followed by activation functions. **Right:** The ReLU function (Regular Linear Unit), which is the most generally used as elementwise nonlinear function (or Activation Function) for machine learning models.

where y is the true label associated with an event (0 if it is noise and 1 if it contains a neutron capture event), and $\tilde{y}$ is the output of the model, normlaized by a sigmoid function to be between 0 and 1.

A.4 Models for further investigations

An interesting class of models that could be developed to get rid of the preselection step (see Section A.5) could be a graph neural network mixed with a time-convolutional neural network or a recurrent neural network, which are two architectures made for dealing with time series.

Time-convolutional neural networks are basically the same as convolutional neural networks presented above, but only in one dimension (time) instead of two (x and y for example for an image). Thus, we could use such networks on the long time series of hits during the $500ms$ after the primary event. However, the function applied to the moving input selected by the kernel would be itself a graph convolutional layer instead of simply a linear function, which would take advantage of both strengths of time-convolutional and graph neural networks.

On the other side, recurrent neural network are another way of dealing with time series. The basic concept is to recursively build an output by feeding successively the data in time-order to the network. This class of networks actually include a wide diversity of models, but they all share this basic concept of recurrence. Then, as well as for the previous method, graph neural convolutional layers can be used to treat the successive inputs.

These methods could not be explored in details in this study, and therefore no precise architecture nor results are presented here. They could however be explored by further studies in the laboratory.

A.5 Preselection

Usual neutron tagging algorithms always include a phase of so called preselection, which consists in applying simple criteria to select the specific small windows on which more developed algorithms (typically machine learning models) will be applied. Furthermore, This preselection allows the selected samples to be well suited for further treatment, which typically includes having enough hits.

An example of common first preselection algorithm is given by the following criteria [5]:

$$N_{10} \geq 7 \qquad N_{10} \leq 50 \qquad N_{200} \leq 200$$

Where N_{10} is the number of hits in a small sliding window of $10ns$, and N_{200} is the number of hits in the $200ns$ window surrounding the $10ns$ window.

The typical expected results after this preselection are 33.2% of efficiency (proportion of remaining neutron events among all the neutron events), and 4.5 mis-tagged background events per neutrino event.

However, other ways of doing preselection exist, as shown in Section 4.6, involving preselecting much more events (and thus much more mis-tagged backgrounds per event), but also much higher preselection efficiency.